

DESIGN, PROTOTYPING AND ANALYSIS OF A LOW-COST DISK PERMANENT MAGNET GENERATOR WITH RECTANGULAR FLAT-SHAPED MAGNETS*

S.M. HOSSEINI,^{1**} M. AGHA-MIRSALIM^{1,2} AND M. MIRZAEI¹

¹Dept. of Electrical Engineering, Amirkabir University of Technology, Tehran, I. R. of Iran

²Dept. of Electrical Engineering, St. Mary's University, San Antonio, TX, USA

Email: m_hosseini@aut.ac.ir

Abstract– This paper presents a new structure to overcome some of the difficulties in axial-flux permanent magnet surface-mounted generators. In the new structure with a non-ferromagnetic holder, the centrifugal force acting on permanent magnets is counteracted. Hence, an increase in the rotation speed and the output power of the generator is feasible. The new design is inexpensive and easy to construct. Thus, by development of the proposed structure, it is possible to construct high-speed, low-cost axial-flux permanent magnet generators.

Keywords– Axial-flux, design, coreless, generator, permanent magnet, prototype, non-ferromagnetic holder

1. INTRODUCTION

Axial-Flux Permanent-Magnet (AFPM) machines with coreless stators are regarded as high efficiency machines for distributed power generation [1-3]. In these machines, the ironless stator avoids the direct magnetic attraction between rotors and stators [2]. Because of the absence of core losses, a generator with this type of design can potentially operate at a higher efficiency than conventional machines [2]. Besides, the compactness and disk-shaped profile make these types of machines particularly suitable for mechanical integration with wind turbines [4].

Electric generators using an axial flux configuration were developed almost 150 years ago. However, their applications have been limited to fractional power due to some difficulties [5], [6]. One major problem is the centrifugal force acting on magnets that tends to move them from their place. Therefore, the rotation speed of AFPM generators is limited, and that leads to using such generators in low-speed applications such as direct coupling with wind turbines [4]. In the past, some researchers have done work on AFPM generators with rated speeds equal to 200 rpm [4] and close to 1950 rpm [7]. In previous AFPM machines, to increase the power output, the pole-numbers were increased, for example, to 28 poles in [4] and 40 in [7]. Another way to reach the desired high outputs is to increase the rotation speed of the AFPM generator with lower pole-numbers. A higher speed leads to higher induced voltage on stator windings. The AFPM generators with no cores always have low inductances [1, 2] and thus current increase does not change the machine performance [8]. One advantage of fewer numbers of magnets is the decrease in the generator cost.

In this paper, after the presentation of the necessary formulas to obtain parameters and the performance of AFPM machines, an axial-flux 3-phase coreless PM generator is designed. This generator has two outer disk rotors and one coreless stator in between. Neodymium-Iron-Boron (Nd-Fe-B) rare-earth

*Received by the editors August 14, 2007; final revised form February 12, 2008.

**Corresponding author

magnets produce the necessary excitation in the generator. These magnets are glued onto the two inner surfaces of rotor disks. After the preliminary design, and for precision study, a two-dimensional (2-D) model of the machine is analyzed using finite element method (FEM) software. From the results of FEM analysis, one can calculate the parameters of the machine. Next, the prototyping procedure of the machine is investigated. In order to counteract the centrifugal forces acting on the magnets of the proposed machine, non-ferromagnetic holders are designed and constructed. Finally, the performance of the machine is obtained with experimental tests. It is expected that by implementing non-ferromagnetic holders, high-speed AFPM generators can be constructed at low costs. By driving the generator at high speeds, higher output power is obtained. For a given frequency, higher speeds result in a lower number of pole-pairs. This decrease lowers the required number of magnets, and consequently, a reduction in the cost is achieved.

2. INTRODUCTION OF THE AXIAL-FLUX PM STRUCTURE WITH CORELESS STATOR

Figure 1 shows the 3-D view of an AFPM machine with two outer rotor disks and one coreless stator in-between. As it can be seen, rectangular flat-shaped high energy Nd-Fe-B magnets are glued onto the inner surfaces of the two rotor disks. The shaft diameter shown in Fig. 1 is not to the scale. It is only to state that the inner diameter of AFPM machine is relatively large.

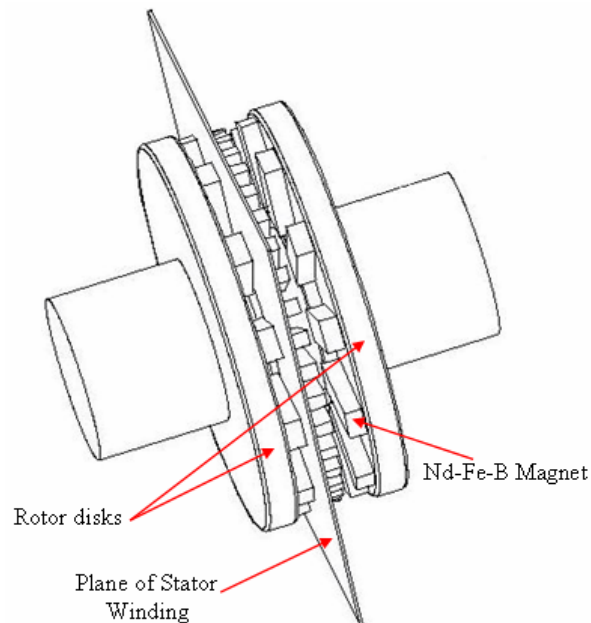


Fig. 1. The structure of the axial flux machine

The rotor poles with an opposite arrangement (N-S type) are shown in Fig. 2. The inner and outer radii of the disk are respectively shown with R_i and R_o in the figure, too. The stator winding of the machine has no iron core and, as shown in Fig. 1, the surface winding of the stator is perpendicular to the machine shaft. There are different methods to do the winding. In this research, the single layer trapezoidal 3-phase winding is used. With this type of winding, only one side of the coil is situated in a special space (or slot in the case of iron-core stator). The typical arrangement for the coils of one phase in a 12-pole pair machine is illustrated in Fig. 3. The other two phases are arranged with ± 120 electrical degrees with respect to the first one.

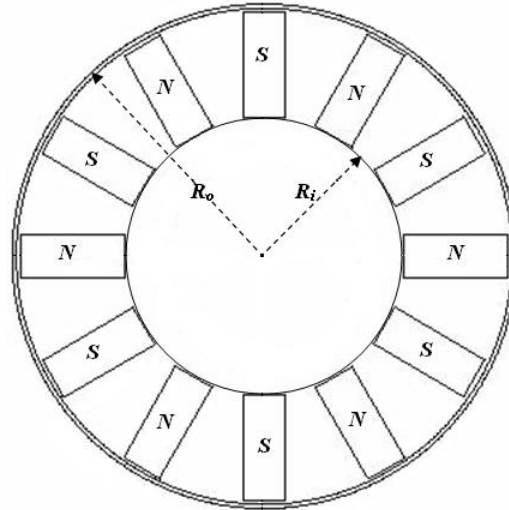


Fig. 2. The arrangements of magnet poles glued onto a rotor surface in a 12-pole pair AFPM machine

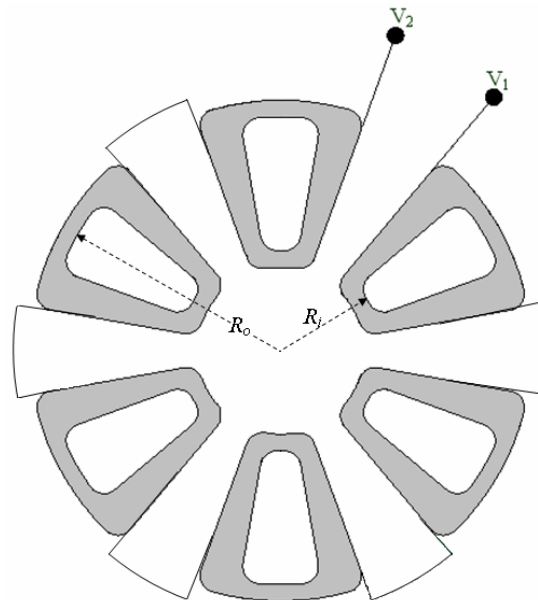


Fig. 3. The arrangements of coils of one phase in a 12-pole pair AFPM machine with single layer trapezoidal winding

3. EQUIVALENT CIRCUIT

The per-phase equivalent circuit of a coreless AFPM machine is shown in Fig. 4a [2]. In this circuit, R_s , L_s , e_m , v_a and i_a are the stator resistance, stator inductance, the induced electromotive force due to the fundamental flux linkages of PMs in the air-gap, the fundamental instantaneous phase voltage and current, respectively. The equivalent resistance of the eddy-current losses of the stator is depicted by R_e .

The synchronous inductance L_s consists of the armature reaction inductance L_a and the total leakage inductance L_l presented as:

$$L_l = L_{lr} + L_{ld} + L_{le} \quad (1)$$

Where, L_{lr} , L_{ld} and L_{le} are the radial leakage inductance, the differential leakage inductance around the radial portions of conductors, and the end winding leakage inductance, respectively. Unlike the

conventional slotted machines, there is no clear definition for leakage and mutual inductances in coreless or slotless machines; therefore it is impossible to express L_{lr} , L_{ld} and L_{le} with exact formulas.

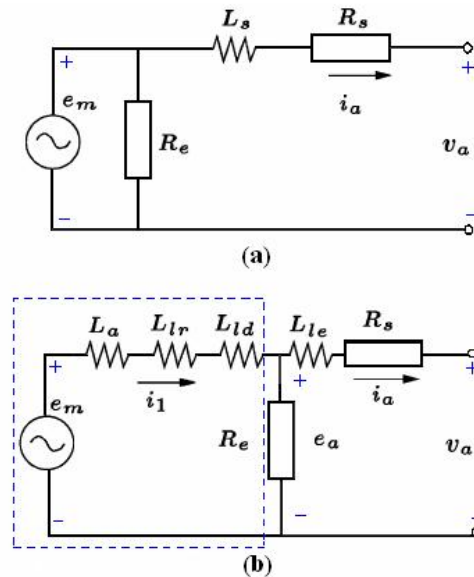


Fig. 4. a) Equivalent circuit, b) Obtained equivalent circuit from 2-D FEM analysis enclosed by the dashed lines

With a 2-D finite element analysis, both the mutual and the leakage flux linkages can be obtained, but not the end winding inductance. To calculate the end winding leakage inductances, several methods have been presented in the literature [1, 2 and 9]. Here in this paper, the method based on the numerical evaluation of the energy stored in the end connections is used [9]. Now, one can divide the synchronous inductance of a coreless machine into $L_a + L_{lr} + L_{ld}$ and the end winding leakage inductance L_{le} .

As an approximation to Fig. 4a, shift R_e to the left of L_{le} . Then, with the 2-D FEM, one can directly calculate all the parameters and quantities of the equivalent circuit enclosed by the dashed lines in Fig. 4b.

4. FEM APPROACH TO CALCULATE INDUCTANCES OF THE EQUIVALENT CIRCUIT

As mentioned before, with the 2-D FEM analysis, both the mutual and the leakage fluxes can be taken into account. The only remaining part is the end winding leakage flux.

The total stator flux of phase windings ψ_{ABC} excluding the end-winding flux leakage, is calculated using the Stokes' theorem [2], i.e.

$$\psi_{ABC} = \int_S \vec{B} \cdot d\vec{s} = \int_S \vec{\nabla} \times \vec{A} \cdot d\vec{s} = \oint_C \vec{A} \cdot d\vec{l}' \quad (2)$$

In this equation, B , A , s , and l' are the flux density, the magnetic vector potential, the surface area of winding, and the length of the outside area, respectively.

As an approximation, the flux linkage of a phase coil can be calculated by working out the difference between the maximum magnetic vector potential values of each coil side. In the case that the coil is not very thin, magnetic vector potential varies in the coil cross-section area. Therefore, the average magnetic vector potential values should be used. For the first order triangular elements, the flux linkage of a coil with N turns, area S and length l is given by [10]:

$$\psi = N \sum_{j=1}^n \frac{\Delta_j}{S} \left[\frac{\zeta}{3} \sum_{i=1}^3 A_{ij} \right] l \quad (3)$$

where A_{ij} is the nodal value of the magnetic vector potential of the triangular element j , $\zeta = +1$ or $\zeta = -1$ indicates the direction of integration either into or out of the plane, Δ_j is the area of the triangular element j and n is the total number of elements of the in-going and out-going areas of the coil. For an AFPM machine that is modeled with only one pole due to symmetry, the total flux linkage of the phase windings is

$$\psi_{ABC} = \frac{2pNl}{a_p S} \sum_{j=1}^u \left[\frac{\Delta_j \zeta}{3} \sum_{i=1}^3 A_{ij} \right] \quad (4)$$

Where u is the total number of elements of the meshed coil areas of the phase in the pole region and a_p is the number of parallel circuits of the stator winding.

To calculate the flux linkage using the FEM, it is necessary to specify the phase current $I = \hat{I} e^{j\phi}$ of the machine. The amplitude of this current may be determined from a given copper loss P_{cu} , which is predetermined based on the thermal analysis of the machine by using:

$$\hat{I} = \sqrt{\frac{2P_{cu}}{3R_s}} = I_q ; (I_d = 0) \quad (5)$$

In which a current angle of $\phi = 90^\circ$ has been assumed for balanced resistive load. With the known current component amplitudes I_d and I_q , the instantaneous three-phase currents i_{abc} , which need to be put in the finite element program according to the rotor position, can be calculated using the inverse Park transformation, i.e.

$$[i_{abc}] = [K_p]^{-1} [i_{dqo}] \quad (6)$$

Where

$$K_p = \frac{2}{3} \begin{bmatrix} \cos \theta & \cos\left(\theta - \frac{2\pi}{3}\right) & \cos\left(\theta + \frac{2\pi}{3}\right) \\ -\sin \theta & -\sin\left(\theta - \frac{2\pi}{3}\right) & -\sin\left(\theta + \frac{2\pi}{3}\right) \\ \frac{1}{2} & \frac{1}{2} & \frac{1}{2} \end{bmatrix} \quad (7)$$

Here, $\theta = \omega t$, and ω is the angular speed of the machine in rad/sec.

Now, by implementing the following relations, the direct and quadrature inductances are obtained as follows:

$$L_{sd} = \frac{\psi_d - \psi_f}{i_d} ; L_{sq} = \frac{\psi_q}{i_q} \quad (8)$$

In (8), ψ_f is the flux produced by magnets.

5. THE EQUIVALENT RESISTANCE OF EDDY-CURRENT LOSS

Magnets produce both axial and tangential components of magnetic fields in the air-gap region. The motion of the magnets over the winding produces alternating fields in the stator conductors in both the axial and the tangential directions. These two fields individually induce eddy currents in the stator windings. If the machine runs at high speeds, the induced eddy currents produce high losses, thus increasing the temperature of the windings and decreasing the efficiency of the machine [10]. Therefore,

the prediction of winding eddy losses with high accuracy is crucial in the design of high-speed AFPM machines.

One of the best methods in the calculation of eddy current losses in the winding of AFPM machines is the multilayer multi-slice method described in [11] and implemented here by the authors. In this method both harmonics of the waveform and its variation with the air-gap position are considered, which is necessary for these types of machines.

6. CALCULATION OF THE END WINDING INDUCTANCE (L_{le}) WITH THE CLASSICAL METHOD

In [8], the analytical method to calculate L_{le} is presented, and the following formula is obtained:

$$L_{le} = 2\mu_0 \frac{N^2 l_{le} \psi_{le}}{pq} \quad (9)$$

Where p , q , and l_{le} are the number of pole pairs, the number of coils per-pole per-phase, and the length of single-sided end connections, respectively, and ψ_{le} can be estimated from the following equation [12]:

$$\psi_{le} \approx 0.3q \quad (10)$$

7. CALCULATION OF EFFICIENCY

By ignoring the losses both in PMs and in the rotor backing steel disks, the input power can be calculated as follows:

$$P_{in} = P_{elm} + \Delta P_{rot} \quad (11)$$

Where P_{elm} is the electromagnetic power, and ΔP_{rot} is the rotational losses that include friction and windage losses, i.e.,

$$\Delta P_{rot} = \Delta P_{fr} + \Delta P_{wind} \quad (12)$$

To calculate the friction losses one can use the empirical relation given in [2], i.e.,

$$\Delta P_{fr} = 0.06 k_{fb} (m_r + m_{sh}) n \quad (13)$$

Where, the shaft friction coefficient, k_{fb} , equals $1.3 \text{ m}^2/\text{s}^2$, and m_r and m_{sh} are the masses of rotor and shaft in kg, respectively, and n is the rotor speed in rpm. Also, the windage losses, ΔP_{wind} , are estimated from the following formula [13]:

$$\Delta P_{wind} = \frac{1}{2} c_f \rho (\pi)^3 (D_{out}^5 - D_{in}^5) \quad (14)$$

Where, c_f , ρ , D_{out} , and D_{in} are the friction coefficient, the density (both for the cooling medium), the outer, and the inner diameters of rotor disks in meters, respectively. Now, the output power is equal to:

$$P_{out} = P_{elm} - \Delta P_R - \Delta P_e \quad (15)$$

Where, ΔP_R and ΔP_e are the Ohmic and eddy losses of stator winding, respectively. The efficiency is then given by $\eta = P_{out} / P_{in}$.

8. DESIGN OF A TYPICAL GENERATOR AND THE CALCULATION OF ITS PARAMETERS

The necessary method and formula to calculate the performance of an AFPM generator has been presented in the previous sections.

Generally, in the design of AFPM machines, the dimensional equations of the machine are related to the choice of objective functions [14]. Here, in the design of the proposed generator, the main goal is to reach maximum output power. To achieve this goal, the following equation is presented [2, 14]:

$$k_d = 1/\sqrt{3} \quad (16)$$

Where $k_d = R_i/R_o$ is the ratio of the machine inner to outer radii. By implementing this ratio and the magnet dimensions given in Table 1, the machine inner and outer radii can be obtained. The results, along with other parameters of the designed machine, are also given in Table 1.

Table 1. Design data

Dimensions of magnets (mm)	25×10×3
B_r (Tesla)	1.2
μ_{rec}	1.045
k_{fb}	1.5
ρ (Kg/m ³)	1.2
Number of pole pairs	12
Speed of rotation (rpm)	3000
Thickness of rotor disk (mm)	10
Air gap distance on one side (mm)	1
Thickness of stator winding (mm)	8
Inner radius (mm)	35
Outer radius (mm)	60
Shaft diameter (mm)	25
Number of phases	3
Number of single-layer coils	18
Diameter of bare wire (mm)	0.4
Number of conductors in each Coil	50
Generator mass (rotors+stator+shaft) (Kg)	3
Current density (A/mm ²)	23.8

For 2-D finite element analysis of a disc generator, first cut the machine through its medium radii and then consider a one pole-pitch of the machine. This analysis does not include end winding connections of the stator windings. The end winding of the stator does not come apart in torque production (motor mode) or voltage induction (generator mode). The end windings just produce Ohmic losses, and the effect is considered in the efficiency calculation of the machine.

With the dimensions of the machine given in Table 1, the 2-D finite element model of the machine is implemented in the finite element software to be analyzed. In Fig. 5, the magnetic flux lines are shown for one pole-pitch of the machine.

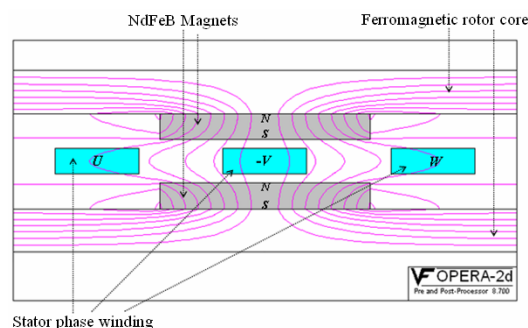


Fig. 5. Magnetic flux lines in one pole-pitch of the machine

Modeling of the air-gap region is done with the Cartesian Air-Gap Element (CAGE) method in [15]. Fig. 6 shows the meshed winding and its layers. The waveforms of axial and tangential components of magnetic fields in different layers are respectively shown in Fig. 7 and Fig. 8.

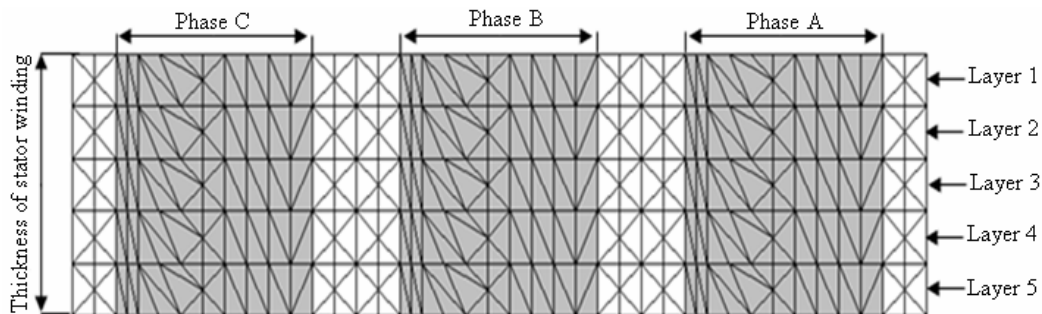


Fig. 6. Schematic of meshed winding and its layers

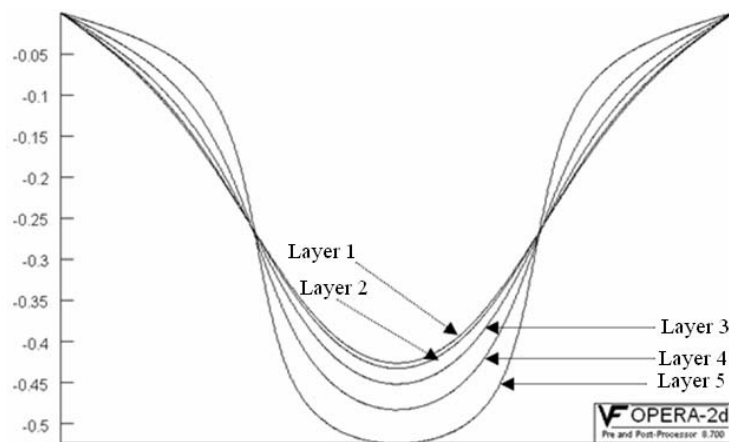


Fig. 7. Waveforms of axial components of magnetic field in different layers

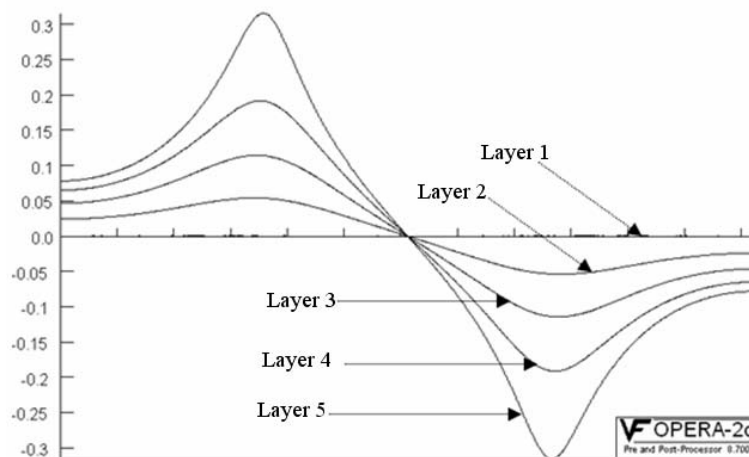


Fig. 8. Waveforms of tangential components of magnetic field in different layers

By Fourier analysis of the waveforms in these figures, the harmonic components are obtained. Then, with the method described in [11], the eddy-current loss is calculated. The parameters of the designed generator are calculated and summarized in Table 2.

Table 2. Characteristics of the designed generator

Speed (rpm)	3000
X_{sd} (Ω)	1.873
X_{sq} (Ω)	1.801
Phase voltage (volt)	56.68
ΔP_e (watt)	1.134
ΔP_R (watt)	51.3
$\cos\Phi$	0.958
Output power (watt)	460
Efficiency (%)	84.3

9. PROTOTYPING AND TESTING OF THE DESIGNED GENERATOR

The centrifugal forces acting on magnets increases as the rotor speed increases, and hence in previous structures of AFPM generators, it was not safe to operate at speeds in excess of 1500 rpm [4, 7].

In this paper a low-cost and simple structure for counteracting the centrifugal forces acting on glued magnets on the rotor disks is designed and named “non-ferromagnetic holder”. The 3-D view of the non-ferromagnetic holder is shown in Fig. 9. This holder is attached to a rotor disc with screws. It is clear that with this provision, magnets cannot move from their places during rotation. Hence, one can increase the speed of the generator to twice the limit used in the previous works. Fig. 10 shows one of the rotor disks with its magnet holders.

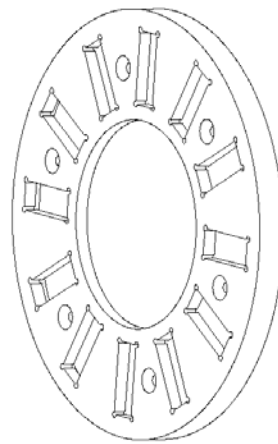


Fig. 9. 3D view of non-ferromagnetic holder

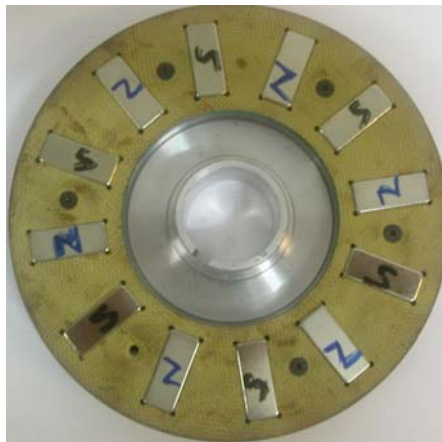


Fig.10. A rotor disk with magnets and non-ferromagnetic holder

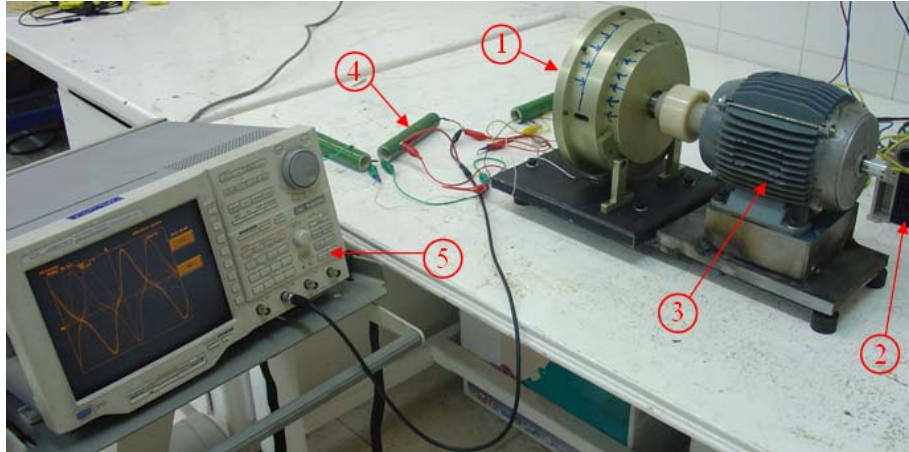


Fig. 11. Test setup (1) Constructed generator (2) Inverter (3) 3-phase induction machine (4) Resistive load (5) Oscilloscope

To experimentally obtain the performance of the generator at different speeds, the speed is changed from zero to the nominal speed of 3000 rpm. Experiments are of two types; no-load and load tests. In the latter cases, three 10- Ω resistive loads are used.

The constructed generator coupled to a 3-phase induction motor is shown in Fig. 11. The speed of the induction motor is changed by a variable frequency inverter. The constructed generator is a relatively small generator. The actual thickness of the generator is demonstrated by the arrows drawn on its frame in Fig. 11.

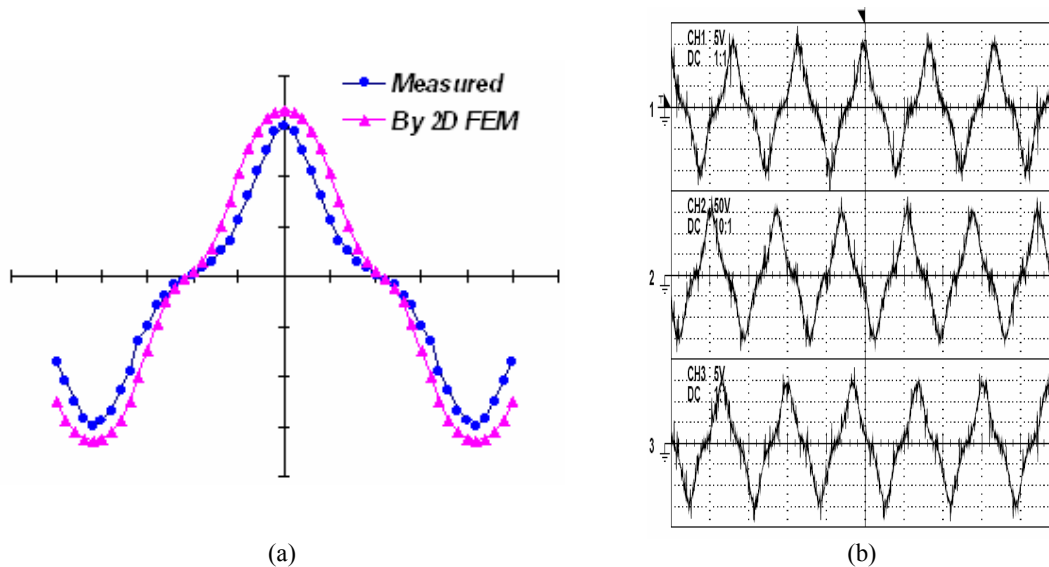


Fig. 12. Waveforms of the predicted and measured output phase voltages at 600 rpm with 10 Ω resistive loads. (a) One phase (b) Three phases

The frequency of the generator at the nominal speed is equal to 300Hz. Fig. 12 shows the waveforms of the output phase voltages at 600 rpm. For the sake of comparison, the predicted waveform is also shown in Fig. 12a.

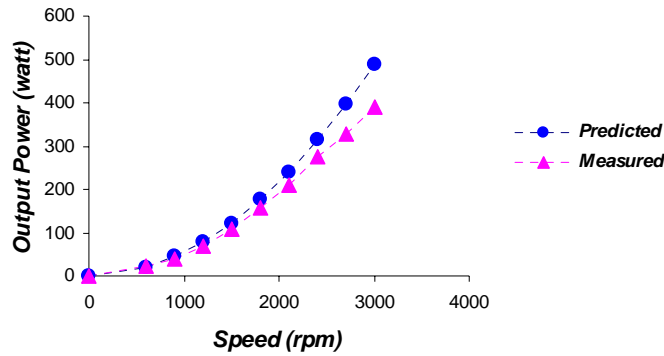


Fig. 13. Variation of both the measured and predicted output powers versus speed

The test results of the generator are given in Table 3. As it is observed in Fig. 12, the output waveform has harmonics. Therefore, only the fundamental component of the output waveform should be used to calculate the output power. The right column in Table 3 shows the peak to peak values of the fundamentals of the output waveforms at different speeds for the load test.

Table 3. The experimental data of the generator

Speed (rpm)	$V_{no-load}^{P-P}$ (V)	$V_{full-load}^{P-P}$ (V)	Peak to peak fundamental component of the output voltage (volt)
600	36	30	25.5
900	50	38	32.3
1200	66	51	43.3
1500	81	63	53.5
1800	97	76	64.5
2100	115.2	88	74.5
2400	130	101	85.5
2700	148	110	93.5
3000	160	120	102

Figure 13 shows both the variations of measured and predicted output powers versus speed. In Fig. 14, the variations of both measured and predicted efficiencies versus speed are depicted. Fig. 14 shows the rise in both output power and efficiency with the increase in speed. The efficiency reaches 78.1% at 3000 rpm. Because of no core losses, the efficiency of the coreless machine is higher than the iron-core machine. The constructed generator is relatively small. From Fig. 14 it is clear that with an increase in speed, the efficiency of the machine increases, but this is not necessarily true for the machine with the iron core.

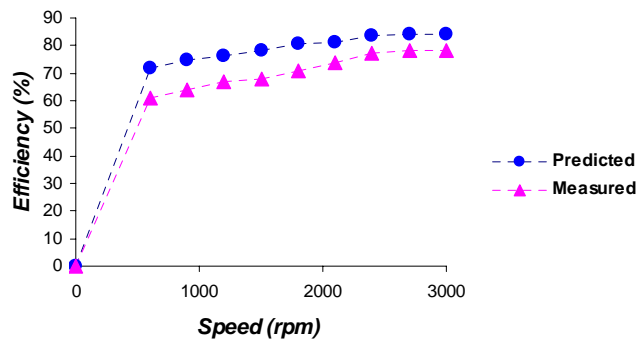


Fig. 14. Variation of both measured and predicted efficiencies versus speed

The experimental characteristics of the prototyped generator are summarized in Table 4.

Table 4. Nominal characteristics of the constructed generator

Output power (watt)	390
Efficiency (%)	78.1
Phase voltage (volt)	40
Phase current (Ampere)	3.6
Frequency (Hertz)	300
X_{sd} (Ω)	2.1
X_{sq} (Ω)	2.1

Major reasons that lead to discrepancies between the theoretical and experimental results might be as follows:

- Using rectangular flat-shaped magnets that produce harmonics in the output voltage [1, 2],
- 2-D finite element analysis, and
- weakening of magnets.

10. CONCLUSION

In this paper, after the introduction of AFPM machines with no iron cores, one typical generator was theoretically designed. Next, with the finite element analysis, the parameters of the generator were calculated. After the construction of the generator, the performance of the generator was experimentally evaluated. AFPM generators are usually driven at low speeds, and hence, to increase the output power, a higher number of pole-pairs is needed. One special characteristic of the designed generator is the use of non-ferromagnetic holders to counteract the centrifugal forces acting on the magnets during the rotation of rotor disks. Hence, it is now possible to drive such machines at high speeds. At these speeds, the output power increases, so there is no need to use more magnets to increase the number of pole-pairs. The prototyped generator is relatively small and cheap. The lower cost might result in the use of these machines in domestic and household appliances too.

REFERENCES

1. Gieras, J. F. & Wing, M. (2002). *Permanent magnet motor technology: design and applications*. 2nd ed. New York: Marcel Dekker.
2. Gieras, J. F., Wang, R. & Kamper, M. J. (2004). *Axial flux permanent magnet brushless machines*. Dordrecht, The Netherlands: Kluwer.
3. Lombard, N. F. & Kamper, M. J. (1999). Analysis and performance of an ironless stator axial flux pm machine. *IEEE Trans. Energy Conversion*, Vol. 14, No. 4, pp. 1051–1056.
4. Chalmers, B. J. & Spooner, E. (1999). An axial-flux permanent-magnet generator for a gearless wind energy system. *IEEE Transactions on Energy Conversion*, Vol. 14, No. 2, pp. 251 – 257.
5. Wallace, R. R., Lipo, T. A., Moran, L. A. & Tapia, J. A. (1997). Design and construction of a permanent magnet axial flux synchronous generator. *Electric Machines and Drives Conference Record, IEEE International* 18-21 May 1997 Page(s): MA1/4.1 - MA1/4.3.
6. Mirzaei, M., Mirsalim, M. & Abdollahi, E. (2007). Analytical modeling of axial air-gap solid rotor induction machines using a quasi-three-dimensional method. *IEEE Transactions on Magnetics*, Vol. 43, No. 7.
7. Wang, R. J., Kamper, M. J., Westhuizen, K. V. D. & Gieras, J. F. (2005). Optimal design of a coreless permanent-magnet generator. *IEEE Transaction on Magnetics*, Vol. 41, No. 1, pp. 55-64.
8. Fitzgerald, A. E. & Kingsley, C. (1961). *Electric machinery*. 2nd ed. New York: McGraw-Hill.

9. Mellara, B. & Santini, R. (1994). FEM computation and optimization of L_d and L_q in disc PM machines. 2nd Int. Workshop on Elect. & Mag. Fields, Leuven, Belgium, paper No. 89.
10. Wang, R. (2003). Design aspects and optimization of an AFPM machine with an ironless stator. Ph.D. dissertation, Dept. of Electrical Engineering, Univ. of Stellenbosch, Matieland, South Africa.
11. Wang, R. J. & Kamper, M. J. (2004). Calculation of eddy current loss in axial field permanent magnet machine with coreless stator. *IEEE Transactions on Energy Conversion*, Vol. 19, No. 3, pp.532-538.
12. Kamper, M. J., Van der Merwe, F. S. & Williamson, S. (1996). Direct finite element design optimization of cage-less reluctance synchronous machine. *IEEE Trans. Energy Conversion*, Vol. 11, No. 3, pp. 547-555.
13. Saari, J. & Arkkio, A. (1994). Losses in high-speed asynchronous motors. in *Proc. ICEM'94*, Vol. 3, Paris, France, pp. 704-708.
14. Aydin, M., Huang, S. & Lipo, T. A. (2004). Axial flux permanent magnet disc machines: A review. SPEEDAM, Capri, Italy.
15. Wang, R., Mohellebi, H., Flack, T. J., Kamper, M. J., Buys, J. & Feliachi, M. (2002). Two dimensional cartesian air-gap element (CAGE) for dynamic finite-element modeling of electrical machines with a flat air-gap. *IEEE Trans. Magnetics*, Vol. 38, pp.1357-1369.